

Quantum information scrambling in strongly disordered Rydberg spin systems

Maximilian Müllenbach,^{1, 2, *} Sebastian Geier,^{2, *} Adrian Braemer,² Eduard Braun,²
Titus Franz,² Gerhard Zürn,² Matthias Weidemüller,² and Martin Gärttner^{3, †}

¹Centre Européen des Sciences Quantiques (CESQ-ISIS, UMR7006),

Université de Strasbourg et CNRS, 23 Rue du Loess, 67200 Strasbourg, France

²Physikalisches Institut, Universität Heidelberg, Im Neuenheimer Feld 226, 69120 Heidelberg, Germany

³Institut für Festkörpertheorie und -optik, Friedrich-Schiller-Universität Jena, Max-Wien-Platz 1, 07743 Jena, Germany

(Dated: December 24, 2025)

Despite the fact that power-law interactions occur in a plethora of physical systems, their many-body dynamics is far less understood than that of nearest-neighbor interacting systems. Here, we study information scrambling in strongly disordered spin systems with power-law interactions via out-of-time-order correlators (OTOCs). Numerically, we find pronounced differences in the dynamical spreading of OTOCs between nearest-neighbor and power-law interacting systems. This deviation persists even for short-range interactions, opposing the common view that these interactions produce dynamics equivalent to the nearest-neighbor case. In a detailed experimental proposal, tailored but not limited to Rydberg tweezer setups, we present a protocol to extract OTOCs in XXZ Heisenberg spin systems with tunable anisotropy and programmable disorder based on currently available techniques.

I. INTRODUCTION

The dynamical evolution of information in quantum many-body systems is the key to understanding many physical phenomena. Questions such as how fast correlations can build up, how hard a system is to simulate classically, and whether thermalization occurs, are intricately linked to the way quantum information spreads [1]. Although the total information entropy is conserved under unitary evolution, information is distributed throughout the system and becomes inaccessible to local probes during the interaction dynamics. This process called scrambling can be captured by the growth of initially local operators [2, 3]. In the Heisenberg picture, the spatiotemporal evolution of an operator \hat{A}_i , acting only on site i at $t = 0$, can be probed by measuring the commutator

$$C(r, t) = \left\| \left[\hat{A}_i(t), \hat{B}_{i+r}(0) \right] \right\|_F^2, \quad (1)$$

where \hat{B}_{i+r} acts on site $i + r$. Here $\|\cdot\|_F^2$ denotes the Frobenius norm, and due to its close connection with the out-of-time-order correlator (OTOC) [2–5] $\langle \hat{A}_i(t) \hat{B}_{i+r}(0) \hat{A}_i(t) \hat{B}_{i+r}(0) \rangle$, $C(r, t)$ is called the out-of-time-order commutator. While there is no universal speed limit for the propagation of information in non-relativistic quantum mechanics, its spread is bounded in short-range interacting systems. Lieb and Robinson (LR) have proven that for finite-range interactions, $C(r, t)$ decays exponentially outside a linear “light cone” $t > r/v$, where v is a system-dependent velocity [4, 6–8]. The LR theorem limits the formation of correlations to a causal region and recently found applications in spectral theory, gate complexity, and in bounding finite-size errors

[9–14]. In disordered systems, the spread of quantum information is slowed down and $C(r, t)$ can be used to discriminate between Anderson [15] and many-body localization (MBL) [16]. Although excitations are localized in both models, the effective $\hat{\tau}_i^z \hat{\tau}_j^z$ interaction of conserved charges in MBL induces dephasing and leads to logarithmic entanglement growth and logarithmic light cones $\ln t \gtrsim r$. [17–27].

Experimental quantum systems, such as Rydberg atoms, trapped ions, NV centers, or nuclear spins in solids (NMR) exhibit long-range power-law interactions $\propto 1/r^\alpha$, which can violate the LR bound. Faster than linear information spreading has been observed, both in theory [28–32] and in experiments [33, 34], for $\alpha < 2d+1$, with d being the spatial dimension of the system under study. The long search for tight and rigorous bounds in power-law interacting systems has only recently been resolved [35–38]. Tight bounds $t \gtrsim r^{\min(\alpha-2d, 1)}$ have been found for $2d < \alpha < 2d+1$, and for $\alpha > 2d+1$, linear light cones have been shown to always be an upper bound [36, 38]. Moreover, the Frobenius norm restricts information spreading to linear light cones already at $\alpha > 5/2$ (in one dimension) for the vast majority of initial states $|\psi\rangle$ [37]. Using quantum typicality and Krylov methods, Luitz and Colmenarez have investigated OTOCs in large ordered Heisenberg systems with power-law interactions [39, 40]. Although they established different short-time scalings $C^{pl}(r, t) \propto t^2/r^{2\alpha}$ for power-law vs. $C^{nn}(r, t) \propto (t^r/r!)^2$ for nearest-neighbor interactions, these can be seen as corrections with magnitudes less than 10^{-4} for dipolar interactions, and the power-law curves quickly merge with the nearest-neighbor results as Jt increases. These recent advances further support the notion that power-law interactions are essentially nearest-neighbor up to small corrections if α is large enough.

In the first part of this work, we show that this expectation fails for strongly disordered systems. To this

* These authors contributed equally to this work.

† Contact author: martin.gaerttner@uni-jena.de

end, we investigate operator growth in the Heisenberg XXZ model with disordered on-site potentials. While for nearest-neighbor interactions, the system exhibits logarithmic light cones $\log t \gtrsim r$, as is characteristic of many-body localization (MBL) [17–27], we numerically find distinctive algebraic light cones for both dipolar ($\alpha = 3$) and van der Waals ($\alpha = 6$) interactions. Identifying the underlying mechanism, we conjecture that this result holds for even larger α for sufficiently strong disorder.

In the second part of this work, we present a protocol for measuring OTOCs in Rydberg atom arrays, implementing Heisenberg XXZ models with tunable anisotropies and on-site disorder [41–46]. One prominent method to extract OTOCs, complementary to randomized measurements [47–49], are echo experiments involving backward evolution $\hat{U}^\dagger = e^{i\hat{H}t}$ [50–61]. However, implementing this time-reversal poses a significant experimental challenge. We propose an efficient Floquet driving that reverses both interactions and disordered potentials. Finally, we investigate different strategies for estimating the relevant infinite temperature expectation values of OTOCs through initial state sampling and compare them under practical experimental considerations.

II. OPERATOR GROWTH IN THE STRONGLY DISORDERED REGIME

A. Model and simulation method

We consider the Heisenberg XXZ model of N interacting spin-1/2 particles on a one-dimensional chain with random on-site potentials.

$$\hat{H} = \frac{1}{2} \sum_{i,j} J_{ij} (\hat{\sigma}_i^x \hat{\sigma}_j^x + \hat{\sigma}_i^y \hat{\sigma}_j^y + \Delta \hat{\sigma}_i^z \hat{\sigma}_j^z) + \sum_i h_i \hat{\sigma}_i^z \quad (2)$$

The coefficients h_i are uniformly drawn from $[-h, h]$, where h denotes the disorder strength. Motivated by NMR spin echo experiments [51, 52], the anisotropy parameter is chosen to be $\Delta = -2$. Interactions J_{ij} are either nearest-neighbor or power-law $J_{ij} = C_\alpha/r^\alpha$. In accordance with the proposed experimental realization (Section III), we focus on dipolar interactions ($\alpha = 3$) but also extend our observations to vdW-interactions. In the case of nearest-neighbor couplings, the Heisenberg XXZ model has been reported to undergo an ergodic to non-ergodic transition at $h_c/|J_z| \approx 3.5$, i.e., $h_c \approx 7$, and exhibit many-body localization [16, 62–65]. We investigate operator growth in the strongly disordered regime ($h = 14$) via the Frobenius norm of out-of-time-order commutators of two Pauli- x operators at distance

$$r = |i - j|$$

$$C_x(r, t) = \|[\hat{\sigma}_i^x(t), \hat{\sigma}_j^x]\|_F^2 \quad (3)$$

$$= \frac{1}{2^N} \text{Tr} ([\hat{\sigma}_i^x(t), \hat{\sigma}_j^x][\hat{\sigma}_i^x(t), \hat{\sigma}_j^x]^\dagger) \quad (4)$$

$$= 2 \left[1 - \text{Re} \left(\frac{1}{2^N} \text{Tr} (\hat{\sigma}_i^x(t) \hat{\sigma}_j^x \hat{\sigma}_i^x(t) \hat{\sigma}_j^x) \right) \right]. \quad (5)$$

We begin by comparing operator growth for nearest-neighbor and dipolar interactions in the strongly-disordered regime. To maximize attainable distances $r = j - i$, we work with open boundary conditions and choose $i = 3$ to avoid influences from reflections at the boundary. The Frobenius norm corresponds to the infinite temperature expectation value and yields the average or *typical* modes of operator growth, while the operator norm, used in the original LR theorem, relates to the fastest mode [40]. There are two computationally costly operations in evaluating Eq. (5): the time evolution and the many matrix-matrix multiplications. We use exact diagonalization to compute the time evolution of $\hat{\sigma}_i^x(t)$ in the Heisenberg picture. To speed up the evaluation of Eq. (5), we rely on the concept of quantum typicality [5, 39, 40], which is a consequence of Lévy's lemma on concentration of measure [66–68]. In high-dimensional Hilbert spaces, infinite-temperature expectation values $1/2^N \text{Tr} \hat{A}$ are well approximated by $\langle \psi | \hat{A} | \psi \rangle$, where $|\psi\rangle$ is a *typical* state, i.e., drawn from the Haar measure. Substituting the trace in Eq. (5) by $\langle \psi | \hat{\sigma}_i^x(t) \hat{\sigma}_j^x \hat{\sigma}_i^x(t) \hat{\sigma}_j^x | \psi \rangle$, we can compute $C_x(r, t)$ by matrix-vector multiplications instead. The error in the approximation decreases exponentially in system size and, depending on system size, averaging over as few as 1 - 100 initial Haar random states (cf. Section III B) gives accurate results. For the system size $N = 13$ used here, we choose to average over 10 states.

B. Algebraic Lightcones

At very strong disorder ($h = 14$), the long-time dynamics of $C_x(r, t)$ differ substantially between power-law and nearest-neighbor interactions. Figure 1 a) showcases the disorder-averaged operator growth $C_x(r, t)$ for both interactions as functions of distance r and (normalized) time Jt , yielding characteristic *light cones*. For nearest-neighbor interactions, we recover the established logarithmic light cones $\ln t \sim r$ (note the logarithmic axis for Jt) for operator growth in the many-body localized regime [17–27]. For dipolar interactions, we see that the operators grow much faster. The contour lines $C_x(r, t_\theta) = \theta$ follow power-law curves $t_\theta \propto r^\beta$. Fitting the tail ($r > 2$) for different thresholds θ , we find $\beta = 1.478 \pm 0.041$, suggesting $\beta \approx \alpha/2$. However, this suggested scaling does not stand up to scrutiny as β/α varies with threshold θ and disorder strength h . Figure 1 b) shows $C_x(r, t)$ as functions of time for different distances $r > 0$, i.e., vertical cuts through the light cones

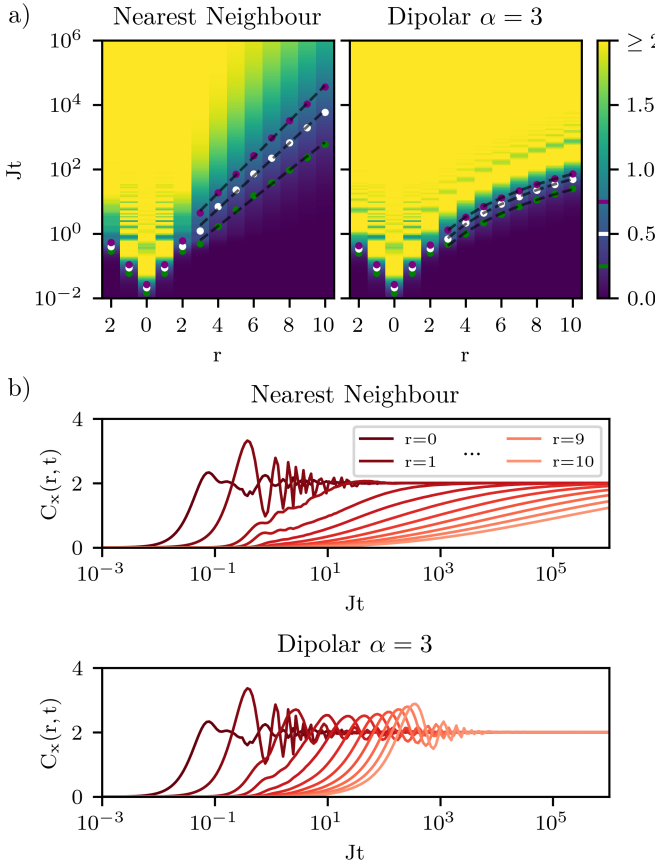


FIG. 1. **Operator growth in the strongly disordered regime.** a) Out-of-time-order commutators $C_x(r, t) = \|\langle \hat{\sigma}_i^x(t) \hat{\sigma}_j^x \rangle\|_F^2$ for the Heisenberg XXZ model with nearest-neighbor or dipolar interactions at strong disorder $h = 14$. Shown is the disorder average over 5000 individual shots at a system size of $N = 13$. The indicated marks correspond to thresholds $C_x(r, t_\theta) = \theta$ with $\theta \in \{0.25, 0.5, 1\}$ and dashed lines are fits $t_\theta \propto e^{\beta r}$, and $t_\theta \propto r^\beta$. b) Vertical cuts through the light cones in (a) showing the time evolution of $C_x(r, t)$ at different distances r .

above in Fig. 1 a). For both types of interaction, we see different phases of growth. $C_x(r, t)$ first grows rapidly, which is especially visible for nearby sites and is consistent with previous short-time calculations [39, 40]. For nearest-neighbor interactions and $r \geq 2$, $C_x(r, t)$ grows more slowly and takes several orders of magnitude longer to reach the saturation value of $C_x = 2$, where OTOCs $\langle \hat{\sigma}_i^x(t) \hat{\sigma}_j^x \hat{\sigma}_i^x(t) \hat{\sigma}_j^x \rangle$ vanish. In the case of dipolar interactions and $r \geq 2$, we find faster operator growth in the second phase and stronger oscillations around $C_x = 2$, which eventually fade out.

To gain a more detailed understanding of the differences between power-law and nearest-neighbor interaction dynamics, it is instructive to investigate the ensemble of individual disorder realizations. In fact, individual disorder realizations feature oscillations for nearest-neighbor interactions, but shot-to-shot they are out of

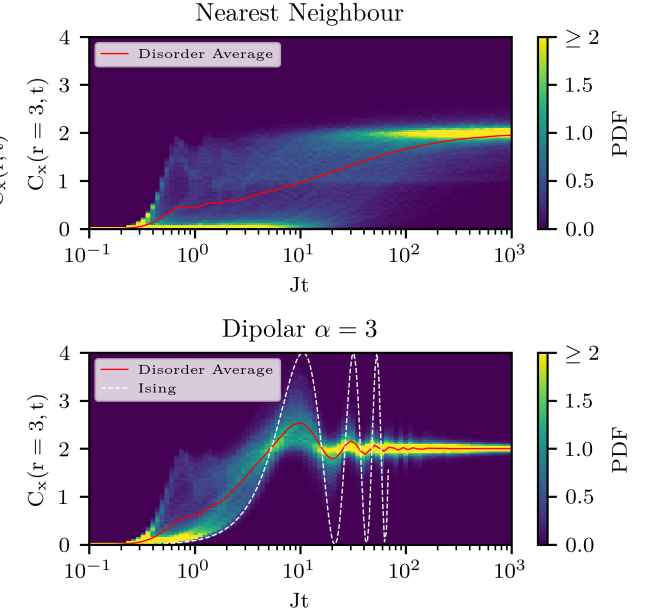


FIG. 2. **Ensemble of Disorder Realizations** Distribution of out-of-time-order commutators $C_x(r, t)$ over 5000 individual disorder realizations ($h = 14$) for nearest-neighbor and dipolar interactions, exemplified for $r = 3$ ($N = 13$). The red curves correspond to the disorder average and the probability of $C_x(r = 3, t)$ to take a given value is indicated by the estimated probability density functions (PDF, color background). The dashed white curve in the lower panel shows the (disorder-independent) analytical solution $C_x^I(r = 3, t)$ for power-law interactions.

phase and average out. In Figure 2, we depict the ensemble of 5000 disorder realizations by plotting the probabilities for $C_x(r = 3, t)$ to assume a given value at time Jt . For both types of interaction, we can observe that the peak of the distribution shifts from $C_x \approx 0$ to $C_x \approx 2$ at late times. As previously noted by Lee et al. [26] for nearest-neighbor interactions, the transfer is not described by a moving unimodal distribution, but shows multimodal behavior. Thus, the disorder average fails to fully portray operator growth in the strongly disordered regime. The left edge of the initial growth phase consists of almost-ordered realizations and displays fast operator growth. Inspecting the distributions, we see that for nearest-neighbor interactions much slower modes of growth are present than for dipolar interactions. These slow modes correspond to realizations where chains of next-neighbor flip-flop exchanges across distance r are heavily suppressed and their extent increases with the disorder strength h . To explain the perceived absence of these slow modes for power-law interactions, we compare with the analytical solution $C_x^I(r, t)$ for the Ising Hamiltonian

$$\hat{H}_I = \frac{1}{2} \sum_{i,j} \frac{C_\alpha}{r^\alpha} \hat{\sigma}_i^z \hat{\sigma}_j^z + \sum_i h_i \hat{\sigma}_i^z. \quad (6)$$

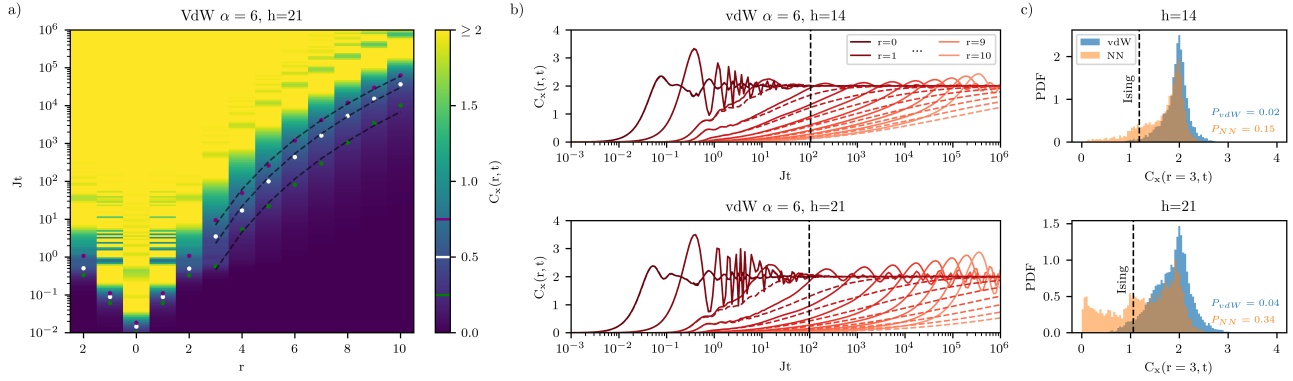


FIG. 3. **Operator Growth for vdW interactions** **a)** Out-of-time-order commutators $C_x(r,t) = \|\hat{[\hat{\sigma}_i^x(t), \hat{\sigma}_j^x]}\|_F^2$ for the Heisenberg XXZ model with vdW interactions at strong disorder $h = 21$. Shown is the disorder average over 5000 individual shots at a system size of $N = 13$. The indicated marks correspond to thresholds $C_x(r,t_\theta) = \theta$ with $\theta \in \{0.25, 0.5, 0.75\}$ and dashed lines are fits $t_\theta \propto e^{\beta r}$. **b)** Time evolutions of $C_x(r,t)$ at different distances r for nearest-neighbor (dashed) and vdW (solid) interactions at $h = 14$ and $h = 21$. The distribution of $C_x(r=3,t)$ sampled across 5000 disorder realizations at $Jt \sim 100$ (vertical dashed line) is illustrated in **c**). The vertical line indicates the value of C_x^I and the fractions of realizations with slower growth are quantified next to the histogram for both types of interactions.

Noting that the interaction and disorder terms commute, we obtain the OTOC $\langle \psi | \hat{U}^\dagger \hat{\sigma}_i^x \hat{U} \hat{\sigma}_j^x \hat{U}^\dagger \hat{\sigma}_i^x \hat{U} \hat{\sigma}_j^x | \psi \rangle = e^{\pm 4J_{ij}t}$ in the computational basis with the sign being $(-)$ for parallel (antiparallel) spins at sites i and j . Thus, taking the infinite-temperature expectation value, the time evolution of $C_x^I(r,t)$ reads

$$C_x^I(r,t) = \|\hat{[\hat{\sigma}_i^x(t), \hat{\sigma}_j^x]}\|_F^2 = 2 - 2 \cos\left(\frac{C_\alpha t}{r^\alpha}\right). \quad (7)$$

and is independent of disorder strength h . This function is shown in white in Fig. 2 for $\alpha = 3$. When the disorder strength h is sufficiently large, the nearest-neighbor model features realizations where operator growth is slower than $C_x^I(r,t)$. For power-law interactions, however, the Ising solution forms a “soft” cutoff, limiting how slow the growth can be. The disorder averages will thus only differ if h is sufficiently large. Additionally, both systems feature oscillations of $C_x(r,t)$ in individual realizations. While for the nearest-neighbor model, they wash out in the disorder average, this cutoff allows them to persist for the power-law system.

The shorter-range the power-law interactions, the higher the disorder strength h must be for a significant difference between the power-law and the nearest-neighbor interacting model. This is because the cutoff is shifted to even slower modes (cf. Eq. (7)). We demonstrate this in Figure 3 for vdW interactions ($\alpha = 6$) with different disorder strengths $h = 14$ and $h = 21$. We recover algebraic light cones and a direct comparison shows that $C_x(r,t)$ deviates less from the corresponding nearest-neighbor case for $h = 14$ than for $h = 21$ and features weaker oscillations. The onset of the oscillations occurs later, as expected from the timescale $r^{-\alpha}$ in Eq. (7). In Fig. 3 c) we plot the distribution of $C_x(r = 3,t)$ at time $Jt \sim 100$ across 5000 disorder realizations to explain the observed deviations by the number of realiza-

tions with growth slower than $C_I(r,t)$. We observe about ~ 10 times more such realizations for nearest-neighbor interactions than for vdW interactions and heavy-tailed or even multimodal distributions. Furthermore, the number of such realizations increases with the disorder strength h . We conclude that unlike ordered spin chains, where corrections are small and short-time, strongly disordered systems exhibit significantly faster operator growth and information spreading between power-law and nearest-neighbor interactions.

III. EXPERIMENTAL PROPOSAL FOR RYDBERG TWEEZER ARRAYS

A. Measurement protocol

Rydberg atom arrays constitute a leading platform for quantum simulation, offering unprecedented control over system geometry and interactions [41, 69, 70]. Despite these capabilities, measuring OTOCs is notoriously difficult due to the need for echo schemes, where both $\hat{U} = e^{-i\hat{H}t}$ and $\hat{U}^\dagger = e^{i\hat{H}t}$ must be implemented. In Rydberg systems, OTOCs have, to the best of our knowledge, only recently been measured in the PXP -model, where time-reversal was implemented on the basis of the Hamiltonian’s particle-hole symmetry via a global σ^z gate [59, 60]. We propose a robust and general scheme to measure OTOCs in tweezer arrays with long-range interactions. We combine recently demonstrated time-reversal techniques [71, 72] with Floquet engineering [42, 43, 73, 74] and the capability to locally manipulate and read out atomic states [46, 75] to extract OTOCs in a broad class of Heisenberg XYZ spin models with tunable anisotropies and with or without additional on-site potentials.

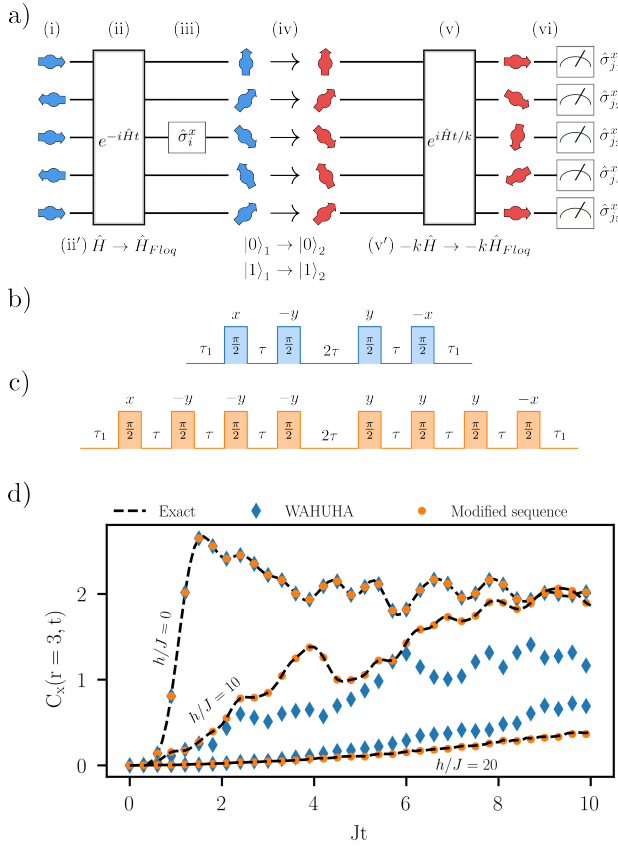


FIG. 4. Measurement Sequence **a)** Sequence of steps for measuring OTOCs. The time-reversal is achieved by transferring the states between two spin-1/2 encodings in the Rydberg manifold, effectively changing C_3 to $-kC_3$. Periodic driving can be applied during forward and backward evolution to realize an effective Floquet Hamiltonian. **b)** The WAHUHA sequence used for introducing $\hat{\sigma}_i^z\hat{\sigma}_j^z$ -interactions to obtain an XXZ model. **c)** Our proposed and modified sequence designed to cancel out fields in x - and y -directions and to implement the XXZ model with random on-site disorder. **d)** Performance of our proposed sequence. We compute the out-of-time-order commutators $C_x(r, t) = \langle \psi | [\hat{o}_3^x(t), \hat{o}_j^x] | \psi \rangle$ exactly (black dashed line) and with Floquet forward and backward propagation for three disorder strengths and a cycle time of $t_c = 0.1J^{-1}$. For comparison, a single, but for both sequences same, disorder realization is used. The initial state is chosen as a Néel state along x , the anisotropy is $\Delta = 0.5$ and system size is $N = 13$.

A variety of Heisenberg Hamiltonians can be implemented by microwave-coupling of different Rydberg states [43–45]. Our mechanism for time-reversal, i.e., changing the sign of the Hamiltonian, relies on the dipolar interaction between Rydberg S - and P -states. Encoding $|0\rangle = |nS\rangle$ and $|1\rangle = |nP\rangle$ as (pseudo-)spins, the system is described by the Heisenberg XX model

$$\hat{H}_{XX} = \frac{1}{2} \sum_{i,j} J_{ij} (\hat{\sigma}_i^x \hat{\sigma}_j^x + \hat{\sigma}_i^y \hat{\sigma}_j^y) \quad (8)$$

with $J_{ij} = C_3(1 - 3\cos^2(\theta_{ij}))/r_{ij}^3$. The sign of C_3 is positive for $\Delta m = 0$ and negative for $\Delta m = \pm 1$, where Δm is the difference in magnetic quantum numbers of the states that encode the two-level system.

The experimental protocol for measuring, for example, a $\hat{\sigma}_i^x\hat{\sigma}_j^x$ -OTOC is shown in Fig. 4 a). In a first step (i), each spin is prepared in an eigenstate $|\psi\rangle$ of $\hat{\sigma}_j^x$. After a forward evolution (ii) up to time t , a π -pulse $R_x(\pi) = -i\hat{\sigma}_i^x$ is applied as a local perturbation (iii) on the atom at site i . Coherently transferring (iv) $|nS\rangle \rightarrow |n'S'\rangle$ and $|nP\rangle \rightarrow |n'P'\rangle$ after a forward evolution up to time t , the interaction coefficient can be changed to $C_3^{(2)} = -kC_3^{(1)}$ with $k = |C_3^{(2)}|/|C_3^{(1)}|$. After a backward evolution (v) up to time $t' = t/k$, the quantum state reads $|\psi(t)\rangle = e^{i\hat{H}t}\hat{\sigma}_i^x e^{-i\hat{H}t}|\psi\rangle$ and the OTOC $\langle \psi | \hat{\sigma}_i^x(t)\hat{\sigma}_j^x\hat{\sigma}_i^x(t)\hat{\sigma}_j^x | \psi \rangle = \pm \langle \psi | \hat{\sigma}_i^x(t)\hat{\sigma}_j^z\hat{\sigma}_i^x(t) | \psi \rangle$ is obtained by a measurement (vi) of $\hat{\sigma}_j^x$.

Using Hamiltonian engineering techniques, inspired by NMR tomography [51, 52], we can modify this protocol to introduce $\hat{\sigma}_i^z\hat{\sigma}_j^z$ interaction terms. To this end, we periodically drive the system with sequences of fast $\pi/2$ -pulses during the forward and backward evolutions. For integer multiples of the cycle time $t = nt_c$, the dynamics is described to lowest order by the Floquet Hamiltonian

$$\hat{H}_{Floq} = \frac{1}{2} \sum_{i,j} J_{ij}^{\perp} (\hat{\sigma}_i^x \hat{\sigma}_j^x + \hat{\sigma}_i^y \hat{\sigma}_j^y) + J_{ij}^{\parallel} \hat{\sigma}_i^z \hat{\sigma}_j^z. \quad (9)$$

Figure 4 b) shows the ubiquitous Waugh-Huber-Haeberlen (WAHUHA) sequence [76], previously used in [42, 72] to create XXZ and, as an extension, XYZ Hamiltonians by changing the delay between the y -pulses as an additional degree of freedom. Given a desired anisotropy $\Delta \in [0, 2]$ and a cycle time t_c , applying WAHUHA with delays of $\tau_1 = \frac{t_c}{2} \frac{2-\Delta}{2+\Delta}$ and $\tau = \frac{t_c}{2} \frac{\Delta}{2+\Delta}$ results in interaction strengths $J_{ij}^{\perp} = J_{ij} \frac{\tau_1 + \tau}{t_c} = J_{ij} \frac{2}{2+\Delta}$ and $J_{ij}^{\parallel} = J_{ij} \frac{2\tau}{t_c} = J_{ij} \frac{2\Delta}{2+\Delta}$. Due to the state transfer, the sign of J_{ij} is changed during the backward evolution and the evolution follows $-k\hat{H}_{Floq}$. This is in contrast to Floquet experiments in NMR, where the starting point is an XXZ Hamiltonian and the Floquet sequence inverts not the sign of the interactions but the sign of the Hamiltonian. A standard WAHUHA sequence in that setting yields $-\frac{1}{5}\hat{H}_{XXZ}$, which results in an experimental duration of $6t$ needed to measure $C_x(r, t)$. Combining state transfer and Floquet engineering allows for a shorter duration of $\frac{2+\Delta}{2}(1 + 1/k)t$ where $k \approx 1$, see [72]. In addition, conventional Floquet time-reversal requires $\Delta = -2$, whereas our scheme unlocks $\Delta \in [0, 2]$.

On-site potentials $h_i\hat{\sigma}_i^z$ can be applied as light shifts from a set of off-resonant optical tweezers. The strength h_i of the potential depends on tweezer intensity and detuning and can be spatially varied as demonstrated in studies on selective light shift addressing [46, 77–79] [80]. However, the WAHUHA sequence introduces unwanted fields of strength $h_i \frac{2\Delta}{2+\Delta}$ in the x - and y -directions, known as chemical shifts [73]. We propose a minimal reflection-

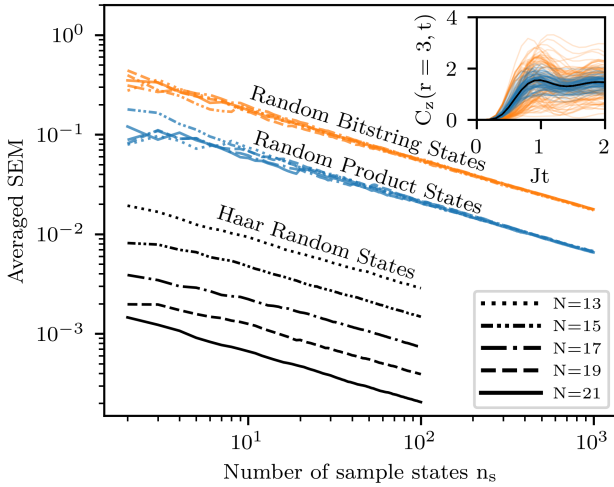


FIG. 5. **Initial State Sampling** Standard error of the mean (SEM) of \bar{C}_z as a function of number of sample states n_s , where \bar{C}_z represents the average of $C_z^\psi(r, t)$ over all distances and 20 timesteps from $Jt = 0.1$ to $Jt = 2$. It is shown for three ensembles of initial states and system sizes $N \in \{13, 15, 17, 19, 21\}$. The inset highlights the variation of $C_z(r = 3, t)$ for distinct initial states $|\psi\rangle$ and uses the same colors for the different ensembles as the main panel.

symmetric sequence, depicted in orange in Fig. 4 c), that eliminates this effect. With $\tau_1 = \frac{t_c}{2} \frac{2-\Delta}{2+\Delta}$ and $\tau = \frac{t_c}{4} \frac{\Delta}{2+\Delta}$, the new sequence results in the same interaction strengths as WAHUHA but in the field strengths $h_i^z = h_i \frac{2-\Delta}{2+\Delta}$ and $h_i^x = h_i^y = 0$. The mechanism of that sequence can be understood by following the Hamiltonian in the toggling frame during the individual stages of the Floquet sequences. Whereas for the WAHUHA sequence the $h_i \hat{\sigma}_i^x$ -fields add $\tau_1 Z \rightarrow \tau Y \rightarrow 2\tau X \rightarrow \tau Y \rightarrow \tau_1 Z$ fields, the total X and Y contributions are nulled in the modified sequence $\tau_1 Z \rightarrow \tau Y \rightarrow \tau X \rightarrow -\tau Y \rightarrow -2\tau X \rightarrow -\tau Y \rightarrow \tau X \rightarrow \tau Y \rightarrow \tau_1 Z$, while the total ratio $J_{ij}^\parallel / J_{ij}^\perp = \Delta$ is kept identical. Because all Hamiltonians in the toggling frame respect the reflection symmetry, i.e., $\tilde{H}_{n+1-k} = \tilde{H}_k$ with n the number of pulses, the first-order correction to \hat{H}_{Floq} vanishes [73], increasing the sequence's robustness. In addition to the new driving sequence, the tweezers must be adjusted after the state transfer to ensure $h'_i = -kh_i$ as the light shift depends on laser intensity and detunings from the respectively used states. In Fig. 4 d), we numerically show that the system driven by the modified sequence at a moderate cycle time of $t_c = 0.1J^{-1}$ faithfully reproduces the evolution of $C_x(r, t)$, whereas WAHUHA fails to follow if disorder is present. For Rydberg atoms at distances of a few μm , interactions are on the order of a few MHz and the required cycle time of $t_c \sim 100$ ns is within the capabilities of current microwave technology.

B. State Sampling Strategies

In Section II, we calculated the infinite-temperature expectation value $2^{-N} \text{Tr}(\hat{W}_i(t) \hat{V}_j \hat{W}_i(t) \hat{V}_j)$ of the OTOC, while in Section III the proposed measurements are with respect to an initial state $|\psi\rangle$. In fact, theoretical works mostly deal with the infinite-temperature state or with bounds on operator growth, whereas most experiments consider more easily producible product states. Furthermore, experiments must deal with the fact that OTOCs are not Hermitian observables. To extract OTOCs, the initial state is as above restricted to an eigenstate of \hat{V}_j so that $\langle \psi | \hat{W}_i(t) \hat{V}_j \hat{W}_i(t) \hat{V}_j | \psi \rangle = \lambda \langle \psi | \hat{W}_i(t) \hat{V}_j \hat{W}_i(t) | \psi \rangle$ as done in [50, 54, 55, 58–60]. Alternatively, a reconstruction from two separate measurements [57, 81] or an interferometric approach [56, 82, 83] have been used in the literature. Additionally, a protocol tailored to OTOCs of Pauli operators that circumvents initial state and ancilla requirements has recently been proposed [84]. The infinite-temperature expectation value is estimated by averaging over many random initial states. In a study on disordered XX-ladder models, Dağ and Duan [85] asked how many Fock states one would need to sample for that. Our goal here is to determine ensembles of initial states that also minimize experimental complexity, namely the difficulty of state preparation and the number of experimental cycles necessary to reach a certain accuracy.

We compare three different ensembles of initial states. While the infinite temperature expectation value of the OTOC can be efficiently calculated with Haar random states, these states are highly-entangled and difficult to prepare experimentally. In addition, the proposed measurement scheme requires that the initial state be an eigenstate of the local operator \hat{V}_j . The states that satisfy this constraint and that are easy to produce are product states $|\psi\rangle = \prod_k |\psi_k\rangle$ where the j th spin is prepared as an eigenstate of \hat{V}_j . We will consider two possibilities here: Random bitstring states and random product states. For the former, every $|\psi_k\rangle$ is initialized in a \hat{V}_k eigenstate, i.e., $|\psi_k\rangle$ is either $|+\rangle_x$ or $|-\rangle_x$ for a $\hat{\sigma}_i^x \hat{\sigma}_j^x$ -OTOC measurement — respectively $|\uparrow\rangle$ or $|\downarrow\rangle$ for a $\hat{\sigma}_i^z \hat{\sigma}_j^z$ -OTOC measurement as below. In contrast, the latter allows any random spin state for a spin at position $k \neq j$ [86].

The inset of Fig. 5 shows the $\hat{\sigma}_i^z \hat{\sigma}_j^z$ -OTOC commutator $C_z(r, t) = \langle \psi | [\hat{\sigma}_i^z(t), \hat{\sigma}_j^z]^\dagger [\hat{\sigma}_i^z(t), \hat{\sigma}_j^z] | \psi \rangle$ for an ordered XXZ Heisenberg chain and the above described classes of initial states. Whereas Haar random states show little variance, C_z depends greatly on the chosen initial state for the more easily preparable product states. The average over many initial states approaches the expectation value $\frac{1}{2^N} \text{Tr}([\hat{\sigma}_i^z(t), \hat{\sigma}_j^z]^\dagger [\hat{\sigma}_i^z(t), \hat{\sigma}_j^z])$, but the speed of convergence differs for different random state ensembles. Samples of random product states show less variance in C_z and their average converges faster than that of random bitstring states. However, random bitstring states have the advantage that the OTOC for all sites j of the

spin chain can be measured simultaneously, while random product states require a series of N measurements. To see which set is better at estimating the infinite-temperature expectation value, we investigate the dependence of the convergence rates on the system size N . We use Krylov methods [5, 39, 40, 87] and restrict calculations to the largest symmetry sector to increase the range of accessible system sizes compared to Section II. At system sizes $N > 13$, calculating the full trace of $[\hat{\sigma}_i^z(t), \hat{\sigma}_j^z]^\dagger [\hat{\sigma}_i^z(t), \hat{\sigma}_j^z]$ proves prohibitively expensive. As a proxy, we use the standard error of the mean (SEM), averaged over time steps from $Jt = 0.1$ to $Jt = 2$, shown in the main panel of Fig. 5. Although random product states converge faster than random bitstring states, the relative error becomes independent of system size as N increases. Because random bitstring states allow for simultaneous readout of N observables, they prove more economical once $N \gtrsim 10$. For Haar random states, we recover the exponential increase in accuracy with system size.

IV. CONCLUSION

Motivated by the capabilities of current quantum simulation platforms, we investigated information scrambling in strongly disordered XXZ Heisenberg chains with power-law interactions. We found algebraic light cones instead of logarithmic light cones that are well-established for the model with nearest-neighbor interactions often used in MBL studies. Although in ordered one-dimensional systems, nearest-neighbor and power-law interactions lead to, up to small corrections, the same operator growth if $\alpha \geq 3$ [38, 39], they significantly differ in strongly disordered systems. Intriguingly, this result holds not just for conventionally long-range dipolar interactions but also for vdW and even shorter-range interactions, which are often approximated as nearest-neighbor. Our results, together with previous studies on “algebraic MBL” [88–93], indicate that complex equilibrium and out-of-equilibrium phenomena induced by long-range interactions [94] can reemerge when disorder, be it

on-site or positional, suppresses otherwise dominant processes. In addition, we proposed an experimental protocol that enables the extraction of OTOCs in a variety of spin models, including XXZ models with tunable anisotropy $0 \leq \Delta < 2$ and programmable disorder. Since the protocol relies on currently available experimental techniques such as Floquet Hamiltonian engineering and state transfer time-reversal, it can readily be applied in analog quantum simulators such as Rydberg or polar molecule tweezer experiments.

ACKNOWLEDGEMENTS

The authors thank J. Schachenmeyer, N. Euler and M. Hornung for helpful discussions. For numerical simulations, we used the Julia programming language [95]. M. Müllenbach acknowledges funding by the European Union H2021 MSCA Doctoral Network QLUSTER (Grant No. 101072964). E. Braun acknowledges support by the IMPRS for Quantum Dynamics in Physics, Chemistry and Biology. This research is supported by funding from the German Research Foundation (DFG) under the project identifier 398816777-SFB 1375 (NOA). The authors acknowledge support by the state of Baden-Württemberg through bwHPC and the German Research Foundation (DFG) through grant no INST 40/575-1 FUGG (JUSTUS 2 cluster). The authors acknowledge support by the state of Baden-Württemberg through bwHPC and the German Research Foundation (DFG) through grant INST 35/1597-1 FUGG (Helix cluster). This work is part of and supported by the Deutsche Forschungsgemeinschaft (DFG, German Research Foundation) under Germany’s Excellence Strategy EXC2181/1-390900948 (the Heidelberg STRUCTURES Excellence Cluster), within the Collaborative Research Centre “SFB 1225 (ISOQUANT)”, the DFG Priority Program “GiRyd 1929”, the Horizon Europe programme HORIZON-CL4-2022-QUANTUM-02-SGA via the project 101113690 (PASQuanS2.1), and the Heidelberg Center for Quantum Dynamics.

[1] R. J. Lewis-Swan, A. Safavi-Naini, A. M. Kaufman, and A. M. Rey, Dynamics of quantum information, *Nature Reviews Physics* **1**, 627 (2019).

[2] B. Swingle, Unscrambling the physics of out-of-time-order correlators, *Nature Physics* **14**, 988 (2018).

[3] S. Xu and B. Swingle, Scrambling Dynamics and Out-of-Time-Ordered Correlators in Quantum Many-Body Systems, *PRX Quantum* **5**, 010201 (2024).

[4] E. H. Lieb and D. W. Robinson, The finite group velocity of quantum spin systems, *Communications in Mathematical Physics* **28**, 251 (1972).

[5] D. J. Luitz and Y. Bar Lev, Information propagation in isolated quantum systems, *Physical Review B* **96**, 020406 (2017).

[6] B. Nachtergael and R. Sims, Much Ado About Something: Why Lieb-Robinson bounds are useful (2011), arXiv:1102.0835.

[7] M. Cheneau, P. Barmettler, D. Poletti, M. Endres, P. Schauß, T. Fukuhara, C. Gross, I. Bloch, C. Kollath, and S. Kuhr, Light-cone-like spreading of correlations in a quantum many-body system, *Nature* **481**, 484 (2012).

[8] C.-F. A. Chen, A. Lucas, and C. Yin, Speed limits and locality in many-body quantum dynamics, *Reports on Progress in Physics* **86**, 116001 (2023).

[9] M. B. Hastings, Lieb-Schultz-Mattis in higher dimensions, *Physical Review B* **69**, 104431 (2004).

[10] S. Bravyi, M. B. Hastings, and F. Verstraete, Lieb-Robinson Bounds and the Generation of Correlations and

Topological Quantum Order, *Physical Review Letters* **97**, 050401 (2006).

[11] M. B. Hastings, An area law for one-dimensional quantum systems, *Journal of Statistical Mechanics: Theory and Experiment* **2007**, P08024 (2007).

[12] M. B. Hastings and S. Michalakis, Quantization of Hall Conductance for Interacting Electrons on a Torus, *Communications in Mathematical Physics* **334**, 433 (2015).

[13] J. Haah, M. B. Hastings, R. Kothari, and G. H. Low, Quantum Algorithm for Simulating Real Time Evolution of Lattice Hamiltonians, *SIAM Journal on Computing*, FOCS18 (2021).

[14] Z. Wang, M. Foss-Feig, and K. R. A. Hazzard, Bounding the finite-size error of quantum many-body dynamics simulations, *Physical Review Research* **3**, L032047 (2021).

[15] P. W. Anderson, Absence of Diffusion in Certain Random Lattices, *Physical Review* **109**, 1492 (1958).

[16] D. A. Abanin, E. Altman, I. Bloch, and M. Serbyn, Colloquium: Many-body localization, thermalization, and entanglement, *Reviews of Modern Physics* **91**, 021001 (2019).

[17] C. K. Burrell and T. J. Osborne, Bounds on the Speed of Information Propagation in Disordered Quantum Spin Chains, *Physical Review Letters* **99**, 167201 (2007).

[18] I. H. Kim, A. Chandran, and D. A. Abanin, Local integrals of motion and the logarithmic lightcone in many-body localized systems (2014), arXiv:1412.3073.

[19] Y. Chen, Universal Logarithmic Scrambling in Many Body Localization (2016), arXiv:1608.02765.

[20] X. Chen, T. Zhou, D. A. Huse, and E. Fradkin, Out-of-time-order correlations in many-body localized and thermal phases, *Annalen der Physik* **529**, 1600332 (2017).

[21] B. Swingle and D. Chowdhury, Slow scrambling in disordered quantum systems, *Physical Review B* **95**, 060201 (2017).

[22] R. Fan, P. Zhang, H. Shen, and H. Zhai, Out-of-time-order correlation for many-body localization, *Science Bulletin* **62**, 707 (2017).

[23] Y. Huang, Y.-L. Zhang, and X. Chen, Out-of-time-ordered correlators in many-body localized systems, *Annalen der Physik* **529**, 1600318 (2017).

[24] R.-Q. He and Z.-Y. Lu, Characterizing many-body localization by out-of-time-ordered correlation, *Physical Review B* **95**, 054201 (2017).

[25] P. Bordia, F. Alet, and P. Hosur, Out-of-time-ordered measurements as a probe of quantum dynamics, *Physical Review A* **97**, 030103 (2018).

[26] J. Lee, D. Kim, and D.-H. Kim, Typical growth behavior of the out-of-time-ordered commutator in many-body localized systems, *Physical Review B* **99**, 184202 (2019).

[27] M. Kim and D.-H. Kim, Slowest and fastest information scrambling in the strongly disordered XXZ model, *Physical Review B* **107**, L220203 (2023).

[28] M. B. Hastings and T. Koma, Spectral Gap and Exponential Decay of Correlations, *Communications in Mathematical Physics* **265**, 781 (2006).

[29] J. Eisert, M. van den Worm, S. R. Manmana, and M. Kastner, Breakdown of Quasilocality in Long-Range Quantum Lattice Models, *Physical Review Letters* **111**, 260401 (2013).

[30] P. Hauke and L. Tagliacozzo, Spread of Correlations in Long-Range Interacting Quantum Systems, *Physical Review Letters* **111**, 207202 (2013).

[31] D. Damanik, M. Lemm, M. Lukic, and W. Yessen, New Anomalous Lieb-Robinson Bounds in Quasiperiodic $\$XY\$$ Chains, *Physical Review Letters* **113**, 127202 (2014).

[32] M. Foss-Feig, Z.-X. Gong, C. W. Clark, and A. V. Gorshkov, Nearly Linear Light Cones in Long-Range Interacting Quantum Systems, *Physical Review Letters* **114**, 157201 (2015).

[33] P. Richerme, Z.-X. Gong, A. Lee, C. Senko, J. Smith, M. Foss-Feig, S. Michalakis, A. V. Gorshkov, and C. Monroe, Non-local propagation of correlations in quantum systems with long-range interactions, *Nature* **511**, 198 (2014).

[34] P. Jurcevic, B. P. Lanyon, P. Hauke, C. Hempel, P. Zoller, R. Blatt, and C. F. Roos, Quasiparticle engineering and entanglement propagation in a quantum many-body system, *Nature* **511**, 202 (2014).

[35] C.-F. Chen and A. Lucas, Finite Speed of Quantum Scrambling with Long Range Interactions, *Physical Review Letters* **123**, 250605 (2019).

[36] T. Kuwahara and K. Saito, Strictly Linear Light Cones in Long-Range Interacting Systems of Arbitrary Dimensions, *Physical Review X* **10**, 031010 (2020).

[37] M. C. Tran, C.-F. Chen, A. Ehrenberg, A. Y. Guo, A. Deshpande, Y. Hong, Z.-X. Gong, A. V. Gorshkov, and A. Lucas, Hierarchy of Linear Light Cones with Long-Range Interactions, *Physical Review X* **10**, 031009 (2020).

[38] M. C. Tran, A. Y. Guo, C. L. Baldwin, A. Ehrenberg, A. V. Gorshkov, and A. Lucas, Lieb-Robinson Light Cone for Power-Law Interactions, *Physical Review Letters* **127**, 160401 (2021).

[39] D. J. Luitz and Y. Bar Lev, Emergent locality in systems with power-law interactions, *Physical Review A* **99**, 010105 (2019).

[40] L. Colmenarez and D. J. Luitz, Lieb-Robinson bounds and out-of-time order correlators in a long-range spin chain, *Physical Review Research* **2**, 043047 (2020).

[41] A. Browaeys and T. Lahaye, Many-body physics with individually controlled Rydberg atoms, *Nature Physics* **16**, 132 (2020).

[42] S. Geier, N. Thaicharoen, C. Hainaut, T. Franz, A. Salzinger, A. Tebben, D. Grimschandl, G. Zürn, and M. Weidmüller, Floquet Hamiltonian engineering of an isolated many-body spin system, *Science* **374**, 1149 (2021).

[43] P. Scholl, H. J. Williams, G. Bornet, F. Wallner, D. Barredo, L. Henriet, A. Signoles, C. Hainaut, T. Franz, S. Geier, A. Tebben, A. Salzinger, G. Zürn, T. Lahaye, M. Weidmüller, and A. Browaeys, Microwave Engineering of Programmable $\$XXZ\$$ Hamiltonians in Arrays of Rydberg Atoms, *PRX Quantum* **3**, 020303 (2022).

[44] L.-M. Steinert, P. Osterholz, R. Eberhard, L. Festa, N. Lorenz, Z. Chen, A. Trautmann, and C. Gross, Spatially Tunable Spin Interactions in Neutral Atom Arrays, *Physical Review Letters* **130**, 243001 (2023).

[45] T. Franz, S. Geier, C. Hainaut, A. Braemer, N. Thaicharoen, M. Hornung, E. Braun, M. Gärttner, G. Zürn, and M. Weidmüller, Observation of anisotropy-independent magnetization dynamics in spatially disordered Heisenberg spin systems, *Physical Review Research* **6**, 033131 (2024).

[46] G. Bornet, G. Emperauger, C. Chen, F. Machado, S. Chern, L. Leclerc, B. Gély, Y. T. Chew, D. Barredo, T. Lahaye, N. Y. Yao, and A. Browaeys, Enhancing a Many-Body Dipolar Rydberg Tweezer Array with Arbitrary Local Controls, *Physical Review Letters* **132**, 263601 (2024).

[47] B. Vermersch, A. Elben, L. M. Sieberer, N. Y. Yao, and P. Zoller, Probing Scrambling Using Statistical Correlations between Randomized Measurements, *Physical Review X* **9**, 021061 (2019).

[48] X. Nie, Z. Zhang, X. Zhao, T. Xin, D. Lu, and J. Li, Detecting scrambling via statistical correlations between randomized measurements on an NMR quantum simulator (2019), arXiv:1903.12237.

[49] M. K. Joshi, A. Elben, B. Vermersch, T. Brydges, C. Maier, P. Zoller, R. Blatt, and C. F. Roos, Quantum Information Scrambling in a Trapped-Ion Quantum Simulator with Tunable Range Interactions, *Physical Review Letters* **124**, 240505 (2020).

[50] M. Gärttner, J. G. Bohnet, A. Safavi-Naini, M. L. Wall, J. J. Bollinger, and A. M. Rey, Measuring out-of-time-order correlations and multiple quantum spectra in a trapped-ion quantum magnet, *Nature Physics* **13**, 781 (2017).

[51] K. X. Wei, C. Ramanathan, and P. Cappellaro, Exploring Localization in Nuclear Spin Chains, *Physical Review Letters* **120**, 070501 (2018).

[52] K. X. Wei, P. Peng, O. Shtanko, I. Marvian, S. Lloyd, C. Ramanathan, and P. Cappellaro, Emergent Prethermalization Signatures in Out-of-Time Ordered Correlations, *Physical Review Letters* **123**, 090605 (2019).

[53] C. M. Sánchez, A. K. Chattah, K. X. Wei, L. Buljubasich, P. Cappellaro, and H. M. Pastawski, Perturbation Independent Decay of the Loschmidt Echo in a Many-Body System, *Physical Review Letters* **124**, 030601 (2020).

[54] X. Nie, B.-B. Wei, X. Chen, Z. Zhang, X. Zhao, C. Qiu, Y. Tian, Y. Ji, T. Xin, D. Lu, and J. Li, Experimental Observation of Equilibrium and Dynamical Quantum Phase Transitions via Out-of-Time-Ordered Correlators, *Physical Review Letters* **124**, 250601 (2020).

[55] S. Pegahan, I. Arakelyan, and J. E. Thomas, Energy-Resolved Information Scrambling in Energy-Space Lattices, *Physical Review Letters* **126**, 070601 (2021).

[56] X. Mi et al., Information scrambling in quantum circuits, *Science* **374**, 1479 (2021).

[57] J. Braumüller, A. H. Karamlou, Y. Yanay, B. Kannan, D. Kim, M. Kjaergaard, A. Melville, B. M. Niedzielski, Y. Sung, A. Vepsäläinen, R. Winik, J. L. Yoder, T. P. Orlando, S. Gustavsson, C. Tahan, and W. D. Oliver, Probing quantum information propagation with out-of-time-ordered correlators, *Nature Physics* **18**, 172 (2022).

[58] S. K. Zhao, Z.-Y. Ge, Z. Xiang, G. M. Xue, H. S. Yan, Z. T. Wang, Z. Wang, H. K. Xu, F. F. Su, Z. H. Yang, H. Zhang, Y.-R. Zhang, X.-Y. Guo, K. Xu, Y. Tian, H. F. Yu, D. N. Zheng, H. Fan, and S. P. Zhao, Probing Operator Spreading via Floquet Engineering in a Superconducting Circuit, *Physical Review Letters* **129**, 160602 (2022).

[59] D.-S. Xiang, Y.-W. Zhang, H.-X. Liu, P. Zhou, D. Yuan, K. Zhang, S.-Y. Zhang, B. Xu, L. Liu, Y. Li, and L. Li, Observation of quantum information collapse-and-revival in a strongly-interacting Rydberg atom array (2024), arXiv:2410.15455.

[60] X. Liang, Z. Yue, Y.-X. Chao, Z.-X. Hua, Y. Lin, M. K. Tey, and L. You, Observation of Anomalous Information Scrambling in a Rydberg Atom Array, *Physical Review Letters* **135**, 050201 (2025).

[61] D. A. Abanin et al., Observation of constructive interference at the edge of quantum ergodicity, *Nature* **646**, 825 (2025).

[62] M. Žnidarič, T. Prosen, and P. Prelovšek, Many-body localization in the Heisenberg XXZ magnet in a random field, *Physical Review B* **77**, 064426 (2008).

[63] A. Pal and D. A. Huse, Many-body localization phase transition, *Physical Review B* **82**, 174411 (2010).

[64] D. J. Luitz, N. Laflorencie, and F. Alet, Many-body localization edge in the random-field Heisenberg chain, *Physical Review B* **91**, 081103 (2015).

[65] D. A. Abanin and Z. Papić, Recent progress in many-body localization, *Annalen der Physik* **529**, 1700169 (2017).

[66] P. Levy, L'addition des variables aléatoires définies sur une circonférence, *Bulletin de la Société Mathématique de France* **67**, 1 (1939).

[67] V. D. Milman and G. Schechtman, *Asymptotic Theory of Finite Dimensional Normed Spaces*, 2nd ed., Lecture Notes in Mathematics No. 1200 (Springer, Berlin ; New York, 2001).

[68] T. Heitmann, J. Richter, D. Schubert, and R. Steinigeweg, Selected applications of typicality to real-time dynamics of quantum many-body systems, *Zeitschrift für Naturforschung A* **75**, 421 (2020).

[69] M. Morgado and S. Whitlock, Quantum simulation and computing with Rydberg-interacting qubits, *AVS Quantum Science* **3**, 023501 (2021).

[70] D. Bluvstein and et al., Logical quantum processor based on reconfigurable atom arrays, *Nature* **626**, 58 (2024).

[71] J.-R. Li, K. Matsuda, C. Miller, A. N. Carroll, W. G. Tobias, J. S. Higgins, and J. Ye, Tunable itinerant spin dynamics with polar molecules, *Nature* **614**, 70 (2023).

[72] S. Geier, A. Braemer, E. Braun, M. Müllenbach, T. Franz, M. Gärttner, G. Zürn, and M. Weidemüller, Time-reversal in a dipolar quantum many-body spin system, *Physical Review Research* **6**, 033197 (2024).

[73] J. Choi, H. Zhou, H. S. Knowles, R. Landig, S. Choi, and M. D. Lukin, Robust Dynamic Hamiltonian Engineering of Many-Body Spin Systems, *Physical Review X* **10**, 031002 (2020).

[74] N. U. Koyluoglu, N. Maskara, J. Feldmeier, and M. D. Lukin, Floquet Engineering of Interactions and Entanglement in Periodically Driven Rydberg Chains, *Physical Review Letters* **135**, 113603 (2025).

[75] T. M. Graham and et al., Multi-qubit entanglement and algorithms on a neutral-atom quantum computer, *Nature* **604**, 457 (2022).

[76] J. S. Waugh, L. M. Huber, and U. Haeberlen, Approach to High-Resolution nmr in Solids, *Physical Review Letters* **20**, 180 (1968).

[77] M. Saffman and T. G. Walker, Analysis of a quantum logic device based on dipole-dipole interactions of optically trapped Rydberg atoms, *Physical Review A* **72**, 022347 (2005).

[78] L. Li, Y. O. Dudin, and A. Kuzmich, Entanglement between light and an optical atomic excitation, *Nature* **498**, 466 (2013).

[79] S. de Léséleuc, D. Barredo, V. Lienhard, A. Browaeys, and T. Lahaye, Optical Control of the Resonant Dipole-

Dipole Interaction between Rydberg Atoms, *Physical Review Letters* **119**, 053202 (2017).

[80] Technically, selective light shift addressing implements $h_i(\hat{\sigma}_i^z + 1)/2$, but the second term can be neglected as it only adds a global phase to the wavefunction.

[81] K. Mitarai and K. Fujii, Methodology for replacing indirect measurements with direct measurements, *Physical Review Research* **1**, 013006 (2019).

[82] B. Swingle, G. Bentsen, M. Schleier-Smith, and P. Hayden, Measuring the scrambling of quantum information, *Physical Review A* **94**, 040302 (2016).

[83] G. Zhu, M. Hafezi, and T. Grover, Measurement of many-body chaos using a quantum clock, *Physical Review A* **94**, 062329 (2016).

[84] M. Kastner, P. Osterholz, and C. Gross, Ancilla-free measurement of out-of-time-ordered correlation functions: General measurement protocol and Rydberg atom implementation, *Physical Review A* **110**, 013303 (2024).

[85] C. B. Dağ and L.-M. Duan, Detection of out-of-time-order correlators and information scrambling in cold atoms: Ladder- XX model, *Physical Review A* **99**, 052322 (2019).

[86] For practical purposes, we generalize this class to fully random product states. We drop the restriction that spin j is in a $\hat{\sigma}_z$ eigenstate to ease averaging over distances and enable the restriction to the largest symmetry sector. Our results remain valid since the performance of such states should be worse than that of fully random product states.

[87] T. J. Park and J. C. Light, Unitary quantum time evolution by iterative Lanczos reduction, *The Journal of Chemical Physics* **85**, 5870 (1986).

[88] N. Y. Yao, C. R. Laumann, S. Gopalakrishnan, M. Knap, M. Müller, E. A. Demler, and M. D. Lukin, Many-Body Localization in Dipolar Systems, *Physical Review Letters* **113**, 243002 (2014).

[89] M. Pino, Entanglement growth in many-body localized systems with long-range interactions, *Physical Review B* **90**, 174204 (2014).

[90] A. L. Burin, Localization in a random XY model with long-range interactions: Intermediate case between single-particle and many-body problems, *Physical Review B* **92**, 104428 (2015).

[91] G. De Tomasi, Algebraic many-body localization and its implications on information propagation, *Physical Review B* **99**, 054204 (2019).

[92] A. Safavi-Naini, M. L. Wall, O. L. Acevedo, A. M. Rey, and R. M. Nandkishore, Quantum dynamics of disordered spin chains with power-law interactions, *Physical Review A* **99**, 033610 (2019).

[93] X. Deng, G. Masella, G. Pupillo, and L. Santos, Universal Algebraic Growth of Entanglement Entropy in Many-Body Localized Systems with Power-Law Interactions, *Physical Review Letters* **125**, 010401 (2020).

[94] N. Defenu, T. Donner, T. Macrì, G. Pagano, S. Ruffo, and A. Trombettoni, Long-range interacting quantum systems, *Reviews of Modern Physics* **95**, 035002 (2023).

[95] J. Bezanson, A. Edelman, S. Karpinski, and V. B. Shah, Julia: A Fresh Approach to Numerical Computing, *SIAM Review* **59**, 65 (2017).